Enhancement of Photocatalytic Activity for Hydrogen Production by Surface Modification of Pt-TiO_2 Nanoparticles with a Double Layer of Photosensitizers

Nobutaka Yoshimura, [a] Atsushi Kobayashi, [a]* Masaki Yoshida, [a] and Masako Kato[a]*

[a] Mr. N. Yoshimura, Dr. A. Kobayashi, Dr. M. Yoshida, and Prof. M. Kato
Department of Chemistry, Faculty of Science,
Hokkaido University
North-10 West-8, Kita-ku, Sapporo 060-0810, Japan
E-mail: akoba@sci.hokudai.ac.jp (A.K.) mkato@sci.hokudai.ac.jp (M. K.)

Supporting information for this article is given via a link at the end of the document.

Abstract: To investigate the effect of the surface structure of dye-sensitized photocatalyst nanoparticles, we prepared three types of Ru(II)-photosensitizer(PS)-double-layered Pt-cocatalyst-loaded TiO_2 nanoparticles with different surface structures, Zr-**RuCP^6**-Zr-**RuP^6**@*N* wt%Pt-TiO_2, **RuCP^6**-Zr-**RuP^6**@*N* wt%Pt-TiO_2, and **RuCP^2**-Zr-**RuP^6**@*N* wt%Pt-TiO_2 (*N* = 0.2, 1, and 5), and evaluated their photocatalytic H_2 evolution activity in the presence of redox-reversible iodide (I^-) as the electron donor. Although the driving force of the electron injection from I^- to the photooxidized Ru(III) PS is comparable, the activity increased in the following order: **RuCP^2**-Zr-**RuP^6**@1 wt%Pt-TiO_2 < **RuCP^6**-Zr-**RuP^6**@1 wt%Pt-TiO_2 < Zr-**RuCP^6**-Zr-**RuP^6**@1 wt%Pt-TiO_2. The apparent quantum yield (AQY) of Zr-**RuCP^6**-Zr-**RuP^6**@1 wt%Pt-TiO_2 in the first hour reached 1%. Zeta potential measurements suggest that the surface Zr^{4+}-phosphate groups attracted I^- anions to the nanoparticle–solution interface. Our results indicate that the surface modification of dye-sensitized photocatalysts is a promising approach to enhance the photocatalytic activity with various redox mediators.

Introduction

"Solar fuel" made using sunlight energy, a sustainable energy source, has attracted considerable attention in recent decades as a promising solution to global warming and the depletion of fossil fuels.[1–5] Photocatalytic water splitting is a simple reaction to produce H_2 as a solar fuel, and, since the discovery of the Honda–Fujishima effect,[6] many studies have been conducted using semiconductor materials[7–12] and perovskite-type composites.[13–15] The sensitization of a semiconductor photocatalyst using a dye, yielding a so-called dye-sensitized photocatalyst (DSP), is a useful strategy to improve the light absorption ability in the visible region by exploiting the absorption bands of the surface-immobilized dye.[16–25] This mechanism is also applicable for Z-scheme water-splitting photocatalysis composed of oxygen- and hydrogen-evolution photocatalysts coupled with a suitable redox mediator.[26–29] To construct highly active Z-scheme water splitting photocatalysts, the charge separation efficiency in the DSP must be improved and the selective recognition of oxidized or reduced mediators is important for achieving one-way electron transfer from the oxygen evolution photocatalyst to hydrogen evolution photocatalyst. Although most studies of DSPs have been conducted in the presence of sacrificial electron donators to promote the water-splitting half reaction,[30–35] there have been several reports concerning water reduction or overall water splitting in the presence of redox-reversible electron mediators.[36,37] In 1993, Mallouk and co-workers achieved an apparent quantum yield (AQY) of 0.3% using a Ru(II) photosensitizer (PS) immobilized on the surface of a water reduction catalyst, $Pt/H_xK_{4-x}Nb_6O_{17}$, using iodide as a redox-reversible electron donor.[38] In 2013, Abe *et al.* reported overall water splitting (AQY = 0.05%) using coumarin derivatives (NKX-2677) immobilized on $Pt/H_xK_{4-x}Nb_6O_{17}$ as a water reduction DSP coupled with an O_2 evolution photocatalyst comprising IrO_2–Pt/WO_3 and iodide redox mediator.[39] Recently, Maeda and co-workers reported a high AQY value (2.4%) for a Z-scheme DSP composed of Ru(II) dye-sensitized $Al_2O_3/Pt/HCa_2Nb_3O_{10}$ nanosheets for water reduction and PtO_x/H–Cs–WO_3 O_2 evolution photocatalyst.[40] These remarkable works suggest that the suppression of the back reaction from the H_2 evolution Pt cocatalyst to the oxidized redox mediator by immobilization of Pt cocatalyst in the interlayer space of layered niobates is a key strategy for achieving electron donation from the redox mediator. However, this approach does not improve the charge separation efficiency between the surface-immobilized PS and redox mediator.

Thus, we have systematically prepared multi-dye-layers on the Pt-cocatalyst-loaded TiO_2 (Pt-TiO_2) nanoparticle surface using phosphonate-functionalized Ru(II)-polypyridyl complexes as photosensitizing dyes with a Zr^{4+} cation binder and found that the photocatalytic H_2 evolution activity is remarkably improved by using multiple layers of the Ru(II) PS.[41,42] Recently, the triple-dye-layered nanoparticle photocatalysts, **RuCP^2**-Zr-**RuP^4**-Zr-**RuP^6**@1 wt%Pt-TiO_2 (**RuCP^2** = $[Ru(bpy)_2(mpbpy)]^{2-}$, **RuP^4** = $[Ru(bpy)(pbpy)_2]^{6-}$, **RuP^6** = $[Ru(pbpy)_3]^{10-}$, bpy = 2,2′-bipyridine, H_4mpbpy = 2,2′-bipyridine-4,4′-bis(methane-phosphonic acid), and H_4pbpy = 2,2′-bipyridine-4,4′-bis(phosphonic acid)) achieved AQYs of 0.1% in the presence of iodide because of the electrostatic interaction between iodide and positively charged nanoparticle surface.[43] This result is remarkable because the H_2 evolution proceeded photocatalytically in the presence of the iodide redox mediator, even though the Pt cocatalyst was simply loaded on the TiO_2 nanoparticle surface.

In this work, to enhance the electron donation from iodide, we focused on the surface structure of the nanoparticle photocatalyst. Specifically, we synthesized two different double-PS-layer Pt-TiO_2 nanoparticles with different surface structures: **RuCP^6**-Zr-**RuP^6**@Pt-TiO_2 having phosphate groups on the

surface and Zr-**RuCP⁶**-Zr-**RuP⁶**@Pt-TiO_2 with Zr^{4+}-phosphate groups on the surface (Schemes 1 and S1 in the electronic supplementary information (ESI)), as well as our previously reported **RuCP²**-Zr-**RuP⁶**@Pt-TiO_2 without any surface phosphonates. The Ru(II) PS **RuCP⁶** immobilized on the outer layer exhibited a comparable Ru(III)/Ru(II) redox potential (1.12 V vs. normal hydrogen electrode (NHE)) to that of previously used **RuCP²** (1.19 V) even though **RuCP⁶** has four more phosphate groups than **RuCP²**. This difference enables us to investigate the effect of the nanoparticle surface on the photocatalytic H_2 evolution activity. Herein, we demonstrate that the activity increases dramatically in the order of **RuCP²**-Zr-**RuP⁶**@Pt-TiO_2 < **RuCP⁶**-Zr-**RuP⁶**@Pt-TiO_2 < Zr-**RuCP⁶**-Zr-**RuP⁶**@Pt-TiO_2, and the AQY value of Zr-**RuCP⁶**-Zr-**RuP⁶**@1 wt%Pt-TiO_2 in the first hour of reaction was 1%.

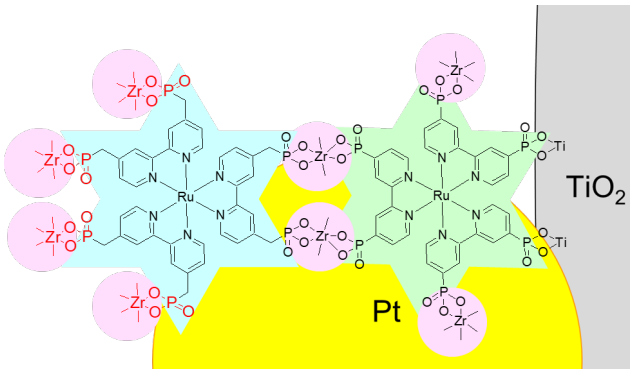

Scheme 1. Schematic structure of double-PS-layer nanoparticle photocatalyst Zr-**RuCP⁶**-Zr-**RuP⁶**@Pt-TiO_2.

Results and Discussion

Characterization of Ru(II)-dye-immobilized Pt-TiO_2 nanoparticles

Figure 1 shows the amount of Ru(II) PS immobilized on the Pt-TiO_2 nanoparticle surface, as estimated from the UV-Vis absorption spectra of the supernatant solutions isolated from the immobilization reaction (see the section titled "Calculation of the amount of Ru(II) complex immobilized on the Pt-TiO_2 nanoparticles," Figure S1 and Table S1 in the ESI). The total amounts of the Ru(II) PS immobilized on the double-PS-layered nanoparticles (**RuY**-Zr-**RuP⁶**@Pt-TiO_2 and Zr-**RuCP⁶**-Zr-**RuP⁶**@Pt-TiO_2, **Y** = **CP²**, **CP⁶**) were more than twice those of single-PS-layered nanoparticles (**RuP⁶**@Pt-TiO_2 and Zr-**RuP⁶**@Pt-TiO_2), indicating that the formation of double-PS-layered structures via Zr^{4+} cation binders is an effective approach to increase the amount of immobilized PS per unit surface area, as we have previously reported.[41–43] The amount in the outer layer of the double-PS-layered nanoparticles strongly depended on the PS, and it decreased on changing **RuCP²** to **RuCP⁶**. Considering that the amount of the PS (**RuP⁶**) immobilized directly on the surface in the inner layer of the Pt-TiO_2 nanoparticles were comparable for all prepared nanoparticles, this trend is attributed to the difference in occupied area between these two Ru(II) PSs with different numbers of phosphonic acid groups; **RuCP²** has only two phosphonic acids and tends to be electrically neutral by releasing two H^+ ions, whereas **RuCP⁶** is a negatively charged molecule on the release of the six H^+ ions from the phosphonic acid groups. As a result, a larger amount of **RuCP²** than **RuCP⁶** was immobilized on the Pt-TiO_2 nanoparticles because of the smaller electrostatic repulsion and molecular size of the former.

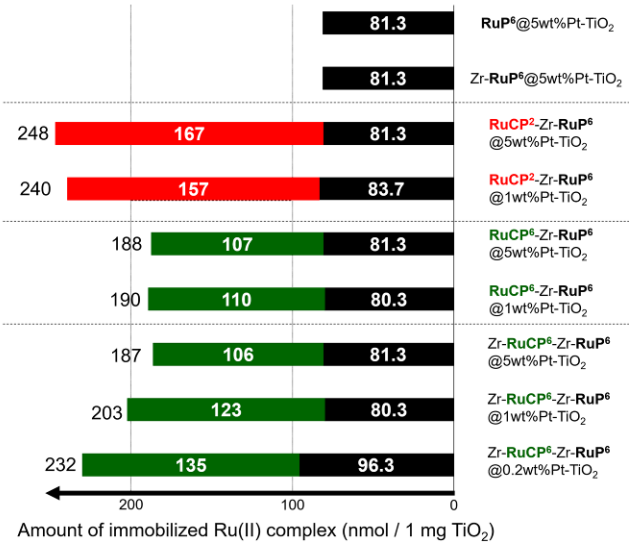

Figure 1. Estimated amounts of the Ru(II) PS (red: **RuCP²**, black: **RuP⁶**, and green: **RuCP⁶**) immobilized on the Pt-TiO_2 nanoparticle surface determined by UV-Vis absorption spectra of the supernatant solutions obtained from the immobilization experiments. Numerical values in each bar show the immobilized amount of Ru(II) PS (nmol /1 mg TiO_2). The total amount of Ru(II) PSs of double-PS-layered nanoparticle is given on the left side of each bar.

The influence of the loading amount of the Pt cocatalyst on the amount of Ru(II) PS immobilized was investigated on the Zr-**RuCP⁶**-Zr-**RuP⁶**@*N* wt%Pt-TiO_2 (*N* = 5, 1, and 0.2) nanoparticles. A negligible difference was observed between the 5 wt% Pt-TiO_2 and 1 wt%Pt-TiO_2, and the same trend was observed for the other nanoparticles (**RuY**-Zr-**RuP⁶**@*N* wt% Pt-TiO_2; **Y** = **CP²**, **CP⁶**). On the other hand, the total amount of immobilized Ru(II) PS in Zr-**RuCP⁶**-Zr-**RuP⁶**@0.2 wt%Pt-TiO_2 was approximately 10% greater than that of the 5 wt%Pt-TiO_2 and 1 wt%Pt-TiO_2 nanoparticles with the same double-PS-layered structure. Considering that the number of Pt colloidal particles in 0.2 wt%Pt-TiO_2 was significantly less than those in 5 wt%Pt-TiO_2 and 1 wt%Pt-TiO_2 (see the section titled "Effect of loaded amount of Pt cocatalyst"), this trend could be because the surfaces of the TiO_2 nanoparticles have a low coverage of colloidal Pt particles. In other words, from the viewpoint of hard-soft acid-base (HSAB) theory, Ru(II) PSs with phosphonates as *hard* bases were preferentially immobilized on the TiO_2 surface with relatively *hard* acids rather than the Pt cocatalyst surface as *soft* acids.

The immobilized amounts of inner **RuP⁶** were estimated to be 80–96 nmol/1 mg TiO_2, and the immobilized amount per unit area of TiO_2 nanoparticle surface was estimated to be 0.078–0.094 nmol·cm^{-2} (Table 1, see the section titled "Calculation of the amount of Ru(II) complex immobilized on the Pt-TiO_2 nanoparticles" in ESI). These are consistent with the calculated value (about 0.083 nmol·cm^{-2}) based on the occupied area of one **RuP⁶** molecule (about 2 nm^2). Thus, these values indicate that the TiO_2 surface should be almost fully covered by **RuP⁶**.

Table 1. Amounts of immobilized Ru(II) complexes on the Pt-TiO_2 nanoparticle surface.

Photocatalyst	Immobilized Ru(II) PS	Amount of immobilized Ru(II) complex (nmol/1 mg TiO_2)[a]	Surface coverage N (nmol / cm^2)
RuP^6@5 wt%Pt-TiO_2	**RuP^6**	81.3	0.0792
Zr-**RuP^6**@5 wt%Pt-TiO_2	**RuP^6**	81.3	0.0792
RuCP^2-Zr-**RuP^6**@5 wt%Pt-TiO_2	inner layer **RuP^6**	81.3	0.0792
	outer layer **RuCP^2**	167	0.163
	Total Ru(II) PS	248	0.241
RuCP^2-Zr-**RuP^6**@1 wt%Pt-TiO_2	inner layer **RuP^6**	83.7	0.0814
	outer layer **RuCP^2**	157	0.153
	Total Ru(II) PS	240	0.233
RuCP^6-Zr-**RuP^6**@5 wt%Pt-TiO_2	inner layer **RuP^6**	81.3	0.0792
	outer layer **RuCP^6**	107	0.104
	Total Ru(II) PS	188	0.183
RuCP^6-Zr-**RuP^6**@1 wt%Pt-TiO_2	inner layer **RuP^6**	80.3	0.0781
	outer layer **RuCP^6**	110	0.107
	Total Ru(II) PS	190	0.185
Zr-**RuCP^6**-Zr-**RuP^6**@5 wt%Pt-TiO_2	inner layer **RuP^6**	81.3	0.0792
	outer layer **RuCP^6**	106	0.0931
	Total Ru(II) PS	187	0.182
Zr-**RuCP^6**-Zr-**RuP^6**@1 wt%Pt-TiO_2	inner layer **RuP^6**	80.3	0.0781
	outer layer **RuCP^6**	123	0.120
	Total Ru(II) PS	203	0.197
Zr-**RuCP^6**-Zr-**RuP^6**@0.2 wt%Pt-TiO_2	inner layer **RuP^6**	96.3	0.0937
	outer layer **RuCP^6**	135	0.131
	Total Ru(II) PS	232	0.226

[a] Estimated based on the absorbance observed in the UV-Vis spectra of each supernatant solution (Figure S1).

In contrast, the total amounts of Ru(II) PS immobilized on double-PS-layered nanoparticles were more than 180 nmol per 1 mg TiO_2 and 0.182 nmol·cm^{-2} per unit area. Thus, **RuP^6** was almost fully immobilized on the TiO_2 surface directly to form the inner PS layer, and the relatively dense outer PS layer was formed by the immobilization of **RuCP^6** on the outer surface of the **RuP^6** inner layer via Zr^{4+} binders. SEM-EDS point analysis suggested that Ru(II) PSs were uniformly immobilized on the TiO_2 surface (Figure S2 and Table S2). We confirmed that the exchange reaction of the inner **RuP^6** by the outer **RuCP^6** did not occur significantly during the preparation of the double-PS-layered **RuCP^6**-Zr-**RuP^6**@5 wt%Pt-TiO_2 because the supernatant solution obtained from the immobilization reaction of **RuCP^6** showed almost identical emission and ^{1}H-NMR spectra and emission decay to those of **RuCP^6** (Figure S3).

X-ray fluorescence (XRF) spectra were recorded to estimate the number of immobilized Zr^{4+} cations (Figure S4). The spectra of all three nanoparticles Zr-**RuCP^6**-Zr-**RuP^6**@5 wt%Pt-TiO_2, **RuCP^6**-Zr-**RuP^6**@5 wt%Pt-TiO_2, Zr-**RuP^6**@5 wt%Pt-TiO_2, and **RuP^6**@5 wt%Pt-TiO_2 contain peaks corresponding to Ti K_α, Ru K_α, and Pt L_α derived from the TiO_2 nanoparticle, Ru(II) PS, and Pt cocatalyst, respectively. The intensities of the Ru K_α radiation of the double-PS-layered nanoparticles were stronger than those of single-PS-layered nanoparticles, which is consistent with the UV-Vis absorption spectra of the supernatants mentioned above. Zr K_α peaks assigned to the Zr^{4+} cations used as the binder between the inner **RuP^6** and outer **RuCP^6** PS layers was also observed, except for **RuP^6**@5 wt%Pt-TiO_2. Notably, the intensity of the Zr K_α peak of Zr-**RuCP^6**-Zr-**RuP^6**@5 wt%Pt-TiO_2 was stronger than that of **RuCP^6**-Zr-**RuP^6**@5 wt%Pt-TiO_2 and Zr-**RuP^6**@5 wt%Pt-TiO_2. This result suggests that the number of immobilized Zr^{4+} cations was increased by the second Zr^{4+} immobilization reaction to form Zr-**RuCP^6**-Zr-**RuP^6**@5 wt%Pt-TiO_2 and also suggests that the surface structure of Zr-**RuCP^6**-Zr-**RuP^6**@5 wt%Pt-TiO_2 is different from that of **RuCP^6**-Zr-**RuP^6**@5 wt%Pt-TiO_2. Further differences between these two nanoparticles were observed in the dynamic light scattering (DLS) measurements in aqueous HCl (pH = 2, Figure S5). The average particle size of **RuCP^6**-Zr-**RuP^6**@5 wt%Pt-TiO_2 with surface phosphonic acids was estimated to be over 1000 nm, whereas that of Zr-**RuCP^6**-Zr-**RuP^6**@5 wt%Pt-TiO_2 with the surface Zr^{4+}-phosphate groups was approximately 500 nm. This difference also suggests a difference in the surface structure; the **RuCP^6**-Zr-**RuP^6**@5 wt%Pt-TiO_2 nanoparticles were easily aggregated by the hydrogen-bonding interactions of the phosphonic acids, whereas the positively charged Zr^{4+}-phosphonate groups on the surface of Zr-**RuCP^6**-Zr-**RuP^6**@5 wt%Pt-TiO_2 could suppress nanoparticle aggregation

because of electrostatic repulsion. All Ru(II)-PS-immobilized Pt-TiO_2 nanoparticles used in this work were found to be non-emissive in the solid state at 298 K, suggesting the electron transfer quenching by TiO_2 is effective not only for the single-PS-layered nanoparticle, but also for the double-PS-layered nanoparticles.

Photocatalytic H_2 evolution reaction

Effect of nanoparticle surface structure

Figure 2 shows the results of photocatalytic H_2 evolution reactions in 0.5 M aqueous KI solutions of three kinds of double-PS-layered nanoparticle photocatalysts with different surface structures: Zr-**RuCP^6**-Zr-**RuP^6**@5 wt%Pt-TiO_2, **RuCP^6**-Zr-**RuP^6**@5 wt%Pt-TiO_2, and **RuCP^2**-Zr-**RuP^6**@5 wt%Pt-TiO_2 in comparison with the single-PS-layered nanoparticles **RuP^6**@5 wt% Pt-TiO_2 and Zr-**RuP^6**@5 wt%Pt-TiO_2. The amount of H_2 produced after 6 h of light irradiation, the turn-over number per PS dye (PS TON), the turn-over frequency per PS dye (PS TOF), and AQY are listed in Table 2. All reactions were conducted in the presence of the same amount Ru(II) PS (100 μM) to keep the same absorbed light intensity under 470 nm excitation that should not excite TiO_2 directly. The amount of H_2 produced after 6 h of light irradiation increased in the following order: **RuP^6**@5 wt%Pt-TiO_2 ≅ Zr-**RuP^6**@5 wt%Pt-TiO_2 < **RuCP^2**-Zr-**RuP^6**@5 wt%Pt-TiO_2 < **RuCP^6**-Zr-**RuP^6**@5 wt%Pt-TiO_2 < Zr-**RuCP^6**-Zr-**RuP^6**@5 wt%Pt-TiO_2. As we previously reported, the photocatalytic H_2 evolution activity was enhanced by the double layering of Ru(II) PS by coordination with Zr^{4+} cations. Notably, the activities of the three kinds of double-PS-layered nanoparticles were significantly different. The estimated PS TON after 6 h irradiation of **RuCP^6**-Zr-**RuP^6**@5 wt%Pt-TiO_2 having surface phosphate groups was 35% higher than that of **RuCP^2**-Zr-**RuP^6**@5 wt%Pt-TiO_2, which lacks surface phosphate groups. This difference is probably due to the reactivity with iodide was

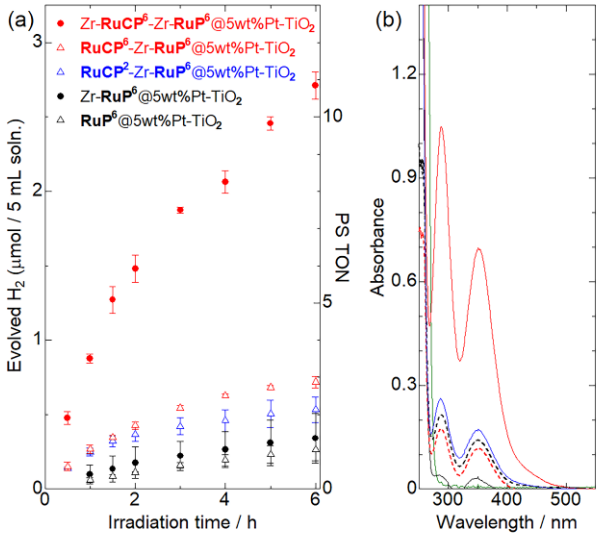

Figure 2. (a) Photocatalytic H_2 evolution reactions driven by Zr-**RuCP^6**-Zr-**RuP^6**@5 wt%Pt-TiO_2 (red closed circles), **RuCP^6**-Zr-**RuP^6**@5 wt%Pt-TiO_2 (red open triangles), **RuCP^2**-Zr-**RuP^6**@5 wt%Pt-TiO_2 (blue open triangles), Zr-**RuP^6**@5 wt%Pt-TiO_2 (black closed circles), and **RuP^6**@5 wt%Pt-TiO_2 (black open symbols) in the presence of 100 μM Ru(II) dye and 0.5 M KI as the electron donor (initial pH = 2.0, λ = 470 ± 10 nm). (b) UV-Vis absorption spectra of the supernatants obtained by centrifugation of the reaction solutions after 6 h irradiation of Zr-**RuCP^6**-Zr-**RuP^6**@5 wt%Pt-TiO_2 (red solid line), **RuCP^6**-Zr-**RuP^6**@5 wt%Pt-TiO_2 (red dashed line), **RuCP^2**-Zr-**RuP^6**@5 wt%Pt-TiO_2 (blue solid line), Zr-**RuP^6**@5 wt%Pt-TiO_2 (black solid line), and **RuP^6**@5 wt%Pt-TiO_2 (black dashed line). Each supernatant (1 mL) was diluted to 20 mL with deionized water before measurement. The green solid line is the spectrum before irradiation.

Table 2. Results of photocatalytic H_2 evolution experiments in aqueous KI.

Photocatalyst	KI (M)	Evolved H_2 (μmol)	Produced I_3^- (μmol)	PS TON[a]	PS initial TOF[b]	PS final TOF[c]	AQY (%)[a]
RuP^6@5 wt%Pt-TiO_2	0.5	0.27	0.37	1.1	0.24	-	<0.01
Zr-**RuP^6**@5 wt%Pt-TiO_2	0.5	0.34	< 0.10	1.4	0.39	0.13	0.011
RuCP^2-Zr-**RuP^6**@5 wt%Pt-TiO_2	0.5	0.53	0.54	2.1	0.99	-	0.018
RuCP^2-Zr-**RuP^6**@1 wt%Pt-TiO_2	0.5	0.84	-	3.4	1.3	0.22	0.028
RuCP^6-Zr-**RuP^6**@5 wt%Pt-TiO_2	0.5	0.72	0.20	2.9	1.1	0.15	0.024
RuCP^6-Zr-**RuP^6**@1 wt%Pt-TiO_2	0.5	8.8	6.2	33.2	8.5	3.6	0.30
RuCP^6-Zr-**RuP^6**@1 wt%Pt-TiO_2	0.02	3.9	-	15.7	3.4	1.8	0.13
RuCP^6-Zr-**RuP^6**@1 wt%Pt-TiO_2	0.02 [d]	2.12	-	8.47	0.93	1.3	0.071
Zr-**RuCP^6**-Zr-**RuP^6**@5 wt%Pt-TiO_2	0.5	2.71	2.4	10.8	3.5	1.0	0.18
Zr-**RuCP^6**-Zr-**RuP^6**@1 wt%Pt-TiO_2	0.5	16.1	9.9	64.5	18.5	5.6	0.54
Zr-**RuCP^6**-Zr-**RuP^6**@0.2 wt%Pt-TiO_2	0.5	6.80	6.0	27.2	8.0	2.2	0.23
Zr-**RuCP^6**-Zr-**RuP^6**@1 wt%Pt-TiO_2	0.02	5.44	1.6	21.8	5.8	2.1	0.18
Zr-**RuCP^6**-Zr-**RuP^6**@1 wt%Pt-TiO_2	0.02 [d]	2.24	1.1	8.98	1.1	-	0.075

[a] After 6-h irradiation. [b] First hour of irradiation. [c] Last hour of irradiation. [d] In 0.5 M phosphate buffer (pH = 2.0) aqueous solution.

improved by the surface phosphate groups of the outer **RuCP^6** PS layer. The slightly negative Ru(III)/Ru(II) redox potential of **RuCP^6** (1.12 V vs. NHE) compared to that of **RuCP^2** (1.19 V vs. NHE) may also contribute to the improvement of the electron transfer between the inner **RuP^6** and outer PS layer (see Scheme S2). More interestingly, the estimated PS TON for Zr-**RuCP^6**-Zr-**RuP^6**@5 wt%Pt-TiO_2 having surface Zr^{4+}-phosphate groups was 3.7-times higher than that of **RuCP^2**-Zr-**RuP^6**@5 wt%Pt-TiO_2. According to the report of Meyer *et al*.,[44] the Ru(III)/Ru(II) redox potential of Ru(II) PS with phosphonic acid groups is shifted positively to less than 0.1 V by immobilization to the TiO_2 surface or by coordination bond formation with Zr^{4+} cations, suggesting that the binding of Zr^{4+} to the phosphonic acid groups of **RuCP^6** PS has little effect on the driving force of the electron donation reaction from the iodide (I_3^- /I^- 0.54 V vs. NHE). Because this slight shift should be too small to enhance the photocatalytic activity more than three-fold, we measured the zeta potentials **of Zr-RuCP^6**-Zr-**RuP^6**@5 wt%Pt-TiO_2 and **RuCP^6**-Zr-**RuP^6**@5 wt%Pt-TiO_2 in HCl aqueous solution (pH = 2) to verify the effect of Zr^{4+} binding on the surface (Table S3). The zeta potential of Zr-**RuCP^6**-Zr-**RuP^6**@5 wt%Pt-TiO_2 was estimated to be +7 mV without KI, and it negatively shifted to −6 mV in the presence of 0.5 M KI. On the other hand, **RuCP^6**-Zr-**RuP^6**@5 wt%Pt-TiO_2, which lacks surface Zr^{4+} cations showed a negative value (−7 mV), even without KI, and it negatively shifted to −12 mV upon the addition of 0.5 M KI. The observed zeta potentials without KI suggest that the structure of the nanoparticle surface was different, probably because of Zr^{4+} binding. The negative shifts in the 0.5 M KI aqueous solution could be ascribed to the attraction of iodide anions to the nanoparticle surface by electrostatic interactions with the surface Zr^{4+} cations in the case of Zr-**RuCP^6**-Zr-**RuP^6**@5 wt%Pt-TiO_2, and by hydrogen-bonding interactions with the surface phosphonic acids for **RuCP^6**-Zr-**RuP^6**@5 wt%Pt-TiO_2. The larger negative shift in the zeta potential by KI addition implies that Zr-**RuCP^6**-Zr-**RuP^6**@5 wt%Pt-TiO_2 nanoparticles attract iodide anions more effectively than **RuCP^6**-Zr-**RuP^6**@5 wt%Pt-TiO_2. UV-Vis absorption spectra of the supernatant solutions after 6-h reaction were measured to verify whether iodide acted as the electron donor for photocatalytic hydrogen production (Figure 2(b)). The two absorption bands (288 and 352 nm) of triiodide (I_3^-) were observed, and the absorbance qualitatively agreed with the amount of evolved hydrogen. No hydrogen evolution was observed without KI or in the dark (Table S4). Thus, in these photocatalytic hydrogen evolution reactions, iodide acted as an electron donor, as we have previously reported. No singlet metal–ligand charge transfer (^{1}MLCT) absorption band of Ru(II) PS was observed for any of the supernatant solutions (Figure S6). In addition, the emission band and ^{1}H signals derived from the desorbed Ru(II) PS from the Pt-TiO_2 nanoparticle surface were hardly observed in emission and ^{1}H NMR spectral measurements, respectively, for the supernatant solutions (Figure S7). These results suggest that the release of the Ru(II) PS from the Pt-TiO_2 nanoparticle surface did not occur sufficiently during the reaction.

Effect of amount of loaded Pt cocatalyst

To reveal the effect of the loading amount of Pt cocatalyst on the double-PS-layered Pt-TiO_2 nanoparticles with different surface structures, three types of double-PS-layered nanoparticles, Zr-**RuCP^6**-Zr-**RuP^6**@*N* wt%Pt-TiO_2, **RuCP^6**-Zr-**RuP^6**@*N* wt%Pt-TiO_2, and **RuCP^2**-Zr-**RuP^6**@*N* wt%Pt-TiO_2, with different Pt loadings (*N* = 0.2, 1, and 5) were prepared. This is important because the Pt cocatalyst loaded on the TiO_2 surface is well known to catalyze not only the proton reduction to form H_2 but also the re-reduction of triiodide by H_2.[39] The results are shown in Figure 3 and Table 2. In all three cases, the amount of H_2 evolved after 6 h of irradiation increased on decreasing the amount of loaded Pt cocatalyst from 5 to 1 wt%, and the trend was remarkable for **RuCP^6**-Zr-**RuP^6**@Pt-TiO_2 and Zr-**RuCP^6**-Zr-**RuP^6**@Pt-TiO_2. Zr-**RuCP^6**-Zr-**RuP^6**@1 wt%Pt-TiO_2 exhibited high activity, and the TOF after the first hour and TON after 6 h irradiation were 18.5 and 64.5, respectively. Notably, the AQY in the first hour of reaction was approximately 1%. Although it gradually decreased after 1.5 h light irradiation, the average AQY for 6 h was 0.54%, which is high compared to those of the recent state-of-the-art dye-sensitized photocatalysts.[29] The average AQY value was 1.8- and 19-times higher than that of **RuCP^6**-Zr-**RuP^6**@1 wt%Pt-TiO_2 having phosphate groups and that of **RuCP^2**-Zr-**RuP^6**@1 wt%Pt-TiO_2 without any surface phosphate groups, respectively. In contrast, the photoactivity of Zr-**RuCP^6**-Zr-**RuP^6**@0.2 wt%Pt-TiO_2 was only 40% that of Zr-**RuCP^6**-Zr-**RuP^6**@1 wt%Pt-TiO_2.

To reveal the origin of this remarkable difference observed with respect the loaded amount of Pt, transmission electron microscopy (TEM) analysis of *N* wt%Pt-TiO_2 nanoparticles was conducted (Figures 3(d–f) and Figure S8). These images clearly indicate that the size of the Pt colloidal particles on the TiO_2 surface were reduced from approximately 5.0 nm for 5 wt%Pt-TiO_2 to about 2.9 nm for 1 wt%Pt-TiO_2. On the other hand, the size of the Pt colloidal particles on 0.2 wt%Pt-TiO_2 was almost comparable (approximately 2.6 nm) to that of 1 wt%Pt-TiO_2, but the number of Pt colloidal particles per unit area was significantly smaller than that of 1 wt%Pt-TiO_2. Considering that Pt colloidal particles catalyze not only the H_2 evolution reaction but also the back reaction, that is, re-reduction of triiodide by H_2, the reason why the 1 wt%Pt-TiO_2 nanoparticles showed higher photoactivity than the 5 wt%Pt-TiO_2 nanoparticles could be that triiodide could not approach the surface of the Pt colloidal particles because of the steric bulk of the double-PS-layered structure. The thickness of the single-PS-layer structure on the TiO_2 surface was evaluated to be approximately 1.5–2 nm based on the molecular size of Ru(II) PS, and the thickness of the double-PS-layer structure including the Zr^{4+}-phosphonate layer should be roughly double (about 3–4 nm) that of the Pt colloid having 1 wt% Pt-TiO_2 (2.9 nm). As a result, the sterically bulky triiodide anion hardly approaches the Pt surface. Further, the thickness of the double-PS-layer structure should increase in order: **RuCP^2**-Zr-**RuP^6**@1 wt%Pt-TiO_2 < **RuCP^6**-Zr-**RuP^6**@1 wt%Pt-TiO_2 < Zr-**RuCP^6**-Zr-**RuP^6**@1 wt%Pt-TiO_2 because of the bulkiness of the surface functional groups (phosphonic acids for **RuCP^6**-Zr-**RuP^6**@1 wt%Pt-TiO_2 and Zr^{4+}-phosphonate for Zr-**RuCP^6**-Zr-**RuP^6**@1 wt%Pt-TiO_2). This order is consistent with the order of the amount of evolved H_2 for the 1 wt% Pt-TiO_2 nanoparticles. In contrast, the lower activity of Zr-**RuCP^6**-Zr-**RuP^6**@0.2 wt%Pt-TiO_2 than Zr-**RuCP^6**-Zr-**RuP^6**@1 wt%Pt-TiO_2 could be because the number of Pt colloidal particles on 0.2 wt%Pt-TiO_2 was too low to accept the excited electrons from the conduction band of TiO_2 nanoparticles.

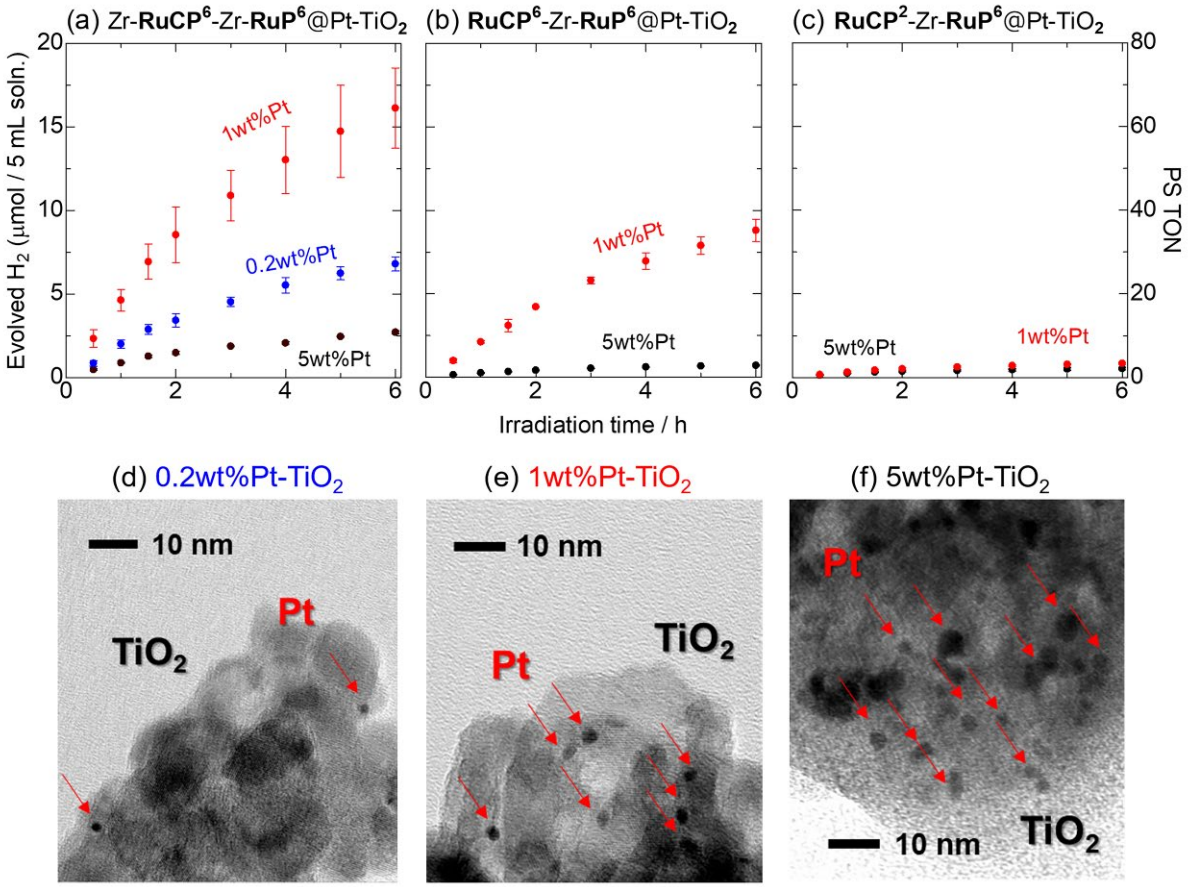

Figure 3. Dependence on the amount of loaded Pt of the photocatalytic H_2 evolution reactions of (a) Zr-**RuCP^6**-Zr-**RuP^6**@Pt-TiO_2, (b) **RuCP^6**-Zr-**RuP^6**@Pt-TiO_2, and (c) **RuCP^2**-Zr-**RuP^6**@Pt-TiO_2 (100 μM Ru(II) dye) in the presence of 0.5 M KI as the electron donor (initial pH = 2.0, λ = 470 ± 10 nm). Black, red, and blue dots represent data for nanoparticles having 5, 1, and 0.2 wt% Pt, respectively. Transmission electron microscopy (TEM) images of (d) 0.2 wt%Pt-TiO_2, (e) 1 wt%Pt-TiO_2, and (f) 5 wt%Pt-TiO_2. Red arrows indicate the Pt cocatalysts loaded on the surface of TiO_2.

The UV-Vis absorption spectra of the supernatant solutions after 6 h irradiation clearly indicate the production of triiodide as the oxidation product of the H_2 evolution reaction (Figure S6), and the produced amount of triiodide qualitatively agreed with that of H_2 evolved (Table 2). The intense absorption band of I_3^- for the reaction solution of Zr-**RuCP^6**-Zr-**RuP^6**@1 wt%Pt-TiO_2 (Figure S6(h)) suggests that the oxidative product I_3^- would interfere the light absorption of Ru(II) PS immobilized on Pt-TiO_2 surface, leading to the gradual decrease of photocatalytic activity (see Figure 3(a)).

Effects of iodide concentration and phosphate pH buffer

To gain further insight into the role of the Zr^{4+}-phosphonate groups of Zr-**RuCP^6**-Zr-**RuP^6**@1 wt%Pt-TiO_2 nanoparticles, the photocatalytic H_2 evolution reaction in the presence of Zr-**RuCP^6**-Zr-**RuP^6**@1 wt%Pt-TiO_2 or **RuCP^6**-Zr-**RuP^6**@1 wt%Pt-TiO_2 was conducted in aqueous phosphate buffer (0.5 M, pH = 2) solution. Because phosphate anions can be expected to coordinate to the surface Zr^{4+} cations of Zr-**RuCP^6**-Zr-**RuP^6**@1 wt%Pt-TiO_2 in a manner similar to that of the phosphonates functionalized on the Ru(II) PS, the coordinated phosphonate anions could change the nanoparticle surface structure considerably. To maintain a constant pH, we reduced the concentration of the KI electron donor from 0.5 M to 20 mM (Figure 4). First, we investigated the effect of the KI concentration without phosphate buffer (initial pH = 2). The TOF of the initial 1 h irradiation decreased to approximately one-third in both Zr-**RuCP^6**-Zr-**RuP^6**@1 wt%Pt-TiO_2 and **RuCP^6**-Zr-**RuP^6**@1 wt%Pt-TiO_2 (TOF = 5.8 and 3.4). These lower activities compared to those in 0.5 M KI are reasonable because triiodide formation should be suppressed at lower iodide concentrations. However, Zr-**RuCP^6**-Zr-**RuP^6**@1 wt%Pt-TiO_2 still showed a higher activity than **RuCP^6**-Zr-**RuP^6**@1 wt%Pt-TiO_2 even at low KI concentrations, suggesting the superior attraction of the surface Zr^{4+} cations for the iodide electron donor. On the other hand, in the presence of phosphate buffer (0.5 M, pH = 2), the photocatalytic activity decreased further than that without phosphate buffer, and the TOF values of these two nanoparticles were estimated to be almost comparable (TOF = 1.1 and 0.93 for Zr-**RuCP^6**-Zr-**RuP^6**@1 wt%Pt-TiO_2 and **RuCP^6**-Zr-**RuP^6**@1 wt%Pt-TiO_2, respectively). The zeta potentials of both Zr-**RuCP^6**-Zr-**RuP^6**@1 wt%Pt-TiO_2 and **RuCP^6**-Zr-**RuP^6**@1 wt%Pt-TiO_2 in the phosphate buffer aqueous solution were negatively shifted to about −25 mV (Table S3), indicating that the nanoparticle surface was effectively surrounded by phosphate anions. Thus, the decrease in the photocatalytic activity of Zr-**RuCP^6**-Zr-**RuP^6**@1 wt%Pt-TiO_2 in the phosphate buffer condition could be due to the surface covering by

electrostatically attracted phosphonate anions that suppress the electron donation from iodide. Meyer *et al.* suggested that, in addition to the iodide that injects an electron to Ru PS, another iodide anion should be close to stabilize the iodine radical generated in the electron injection; they also demonstrated that hydrogen-bonding interactions with iodide by amide and amino functional groups is effective in improving electron injection.[45-47] In our Zr-**RuCP^6**-Zr-**RuP^6**@1 wt%Pt-TiO_2 nanoparticles, the surface Zr^{4+}-phosphate groups could attract iodide anions near the surface, probably by electrostatic interactions, leading to enhanced H_2 evolution photocatalytic activity.

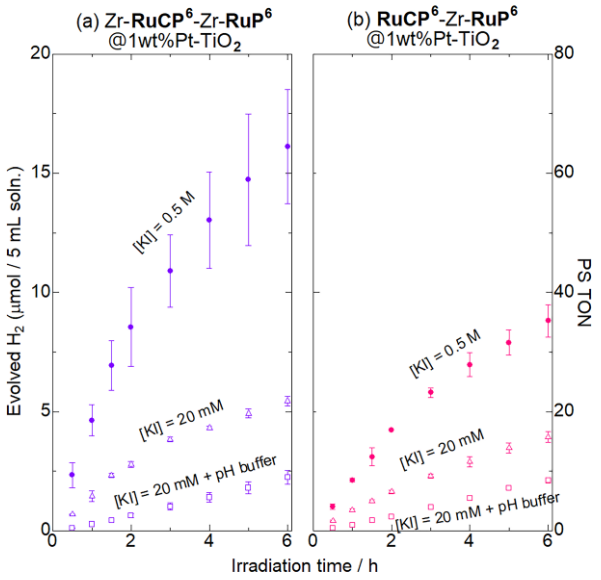

Figure 4. The effects of initial KI concentration and phosphate buffer on the photocatalytic H_2 evolution reaction driven by (a) Zr-**RuCP^6**-Zr-**RuP^6**@1 wt%Pt-TiO_2 and (b) **RuCP^6**-Zr-**RuP^6**@1 wt%Pt-TiO_2 (100 μM Ru(II) dye). Closed circles show the results in 0.5 M KI without pH buffer (the initial pH = 2.0, the same data shown in Figures 3(a) and 3(b)), and open triangles and squares are the results obtained in the 0.02 M KI without and with phosphate pH buffer, respectively (pH = 2.0, λ = 470 ± 10 nm).

Conclusion

To promote electron injection from the redox mediator to the photosensitizer (PS), we prepared three types of Pt-cocatalyst-loaded TiO_2 nanoparticles (*N* wt% Pt-TiO_2, *N* = 0.2, 1, and 5) photocatalysts with double-layered Ru(II) PSs: Zr^{4+}-phosphonate-exposed type nanoparticles (Zr-**RuCP^6**-Zr-**RuP^6**@*N* wt%Pt-TiO_2), phosphonic acid-exposed type nanoparticles (**RuCP^6**-Zr-**RuP^6**@*N* wt%Pt-TiO_2), and bipyridine-exposed nanoparticles (**RuCP^2**-Zr-**RuP^6**@*N* wt%Pt-TiO_2). In aqueous solutions of potassium iodide as a redox-reversible electron donor, the amount of evolved H_2 increased in order **RuCP^2**-Zr-**RuP^6**@*N* wt%Pt-TiO_2 < **RuCP^6**-Zr-**RuP^6**@*N* wt%Pt-TiO_2 < Zr-**RuCP^6**-Zr-**RuP^6**@*N* wt%Pt-TiO_2 (*N* = 1, 5), despite the fact that the driving force for electron injection from I^- to the photooxidized Ru(III) PS is comparable between the three nanoparticles. The highest performance was observed for Zr-**RuCP^6**-Zr-**RuP^6**@1 wt%Pt-TiO_2, which showed an apparent quantum yield of 1% in the first hour of the reaction. TEM analysis revealed that a comparable number of Pt colloidal particles were loaded on both 1 and 5 wt% Pt-TiO_2, but the size of the Pt colloidal particles of 1 wt% Pt-TiO_2 (ca. 2.9 nm) was remarkably smaller than that of 5 wt% Pt-TiO_2 (ca. 5.0 nm) and the thickness of the double-PS-layered **RuCP^6**-Zr-**RuP^6** structure (ca. 4 nm). Thus, the higher activity observed for double-PS-layered 1 wt% Pt-TiO_2 could be due to the suppression of back electron transfer from the Pt cocatalyst to triiodide (I_3^-) by the steric hindrance of the double-PS-layer, as well as the higher activity of the smaller Pt colloidal particles for H_2 evolution. The negative shift in the zeta potential in the iodide aqueous solution suggests that Zr^{4+} ions and phosphonic acid attracted iodide anions to the nanoparticle surface, promoting electron donation to the photooxidized Ru(III) PSs. These results clearly indicate that the surface structure of dye-sensitized nanoparticles has a great influence on the reactivity with the redox mediator. In other words, the reactivity could be modified by changing the functional group of the photosensitizers immobilized on the outer surface. Further studies focusing on the surface structure to regulate the reactivity with various redox mediators is now in progress.

Experimental Section

Materials and syntheses

Caution! *Although we did not encounter any difficulties, most of the chemicals used in this study are potentially harmful and should be used in small quantities and handled with care in a fume hood.* All commercially available starting materials were used as received without further purification. TiO_2 nanoparticles (SSP-M, approximately 15 nm in diameter) were purchased from Sakai Chemical Industry Co. Ltd. The Pt-cocatalyst-loaded TiO_2 nanoparticles were prepared using a previously reported photodeposition method.[48] Ru(II) molecular photosensitizers (**RuCP^2**, **RuCP^6**, and **RuP^6**) were synthesized using previously reported methods.[44,49]

Preparation of Ru(II)-dye-immobilized Pt-TiO_2 nanoparticles

Ru(II)-dye-immobilized Pt-TiO_2 nanoparticles were synthesized with reference to our previous report and prepared by changing the Ru(II) dye. The amount of the Ru(II) dye immobilized on the Pt-TiO_2 nanoparticle surface was estimated using XRF spectroscopy and UV-Vis absorption spectroscopy of the supernatant solution (see Figure S1, Table S1, and the "Calculation of the amount of Ru(II)complex immobilized on the Pt-TiO_2 nanoparticles" section of the ESI). The loaded amounts of Pt cocatalyst on 5 wt% Pt-TiO_2, 1 wt% Pt-TiO_2, and 0.2 wt% Pt-TiO_2 nanoparticles were estimated by XRF spectra to be 5.17, 0.99, and 0.2 wt%, respectively.

Measurements

^{1}H-NMR spectra at room temperature were recorded on an ECZ-400S NMR spectrometer. UV−Vis absorption spectra were recorded using a Shimadzu UV-2400PC spectrophotometer. Luminescence spectra were recorded using a JASCO FP-8600 spectrofluorometer. Emission lifetime measurements were conducted using a Quantaurus-Tau C11367 (Hamamatsu Photonics K. K.) excited by a UV light emitting diode (LED) light source (λ_{ex} = 280 nm). Energy-dispersive XRF spectra were recorded using a Bruker S2 PUMA analyzer. Powder X-ray diffraction studies were conducted using a Rigaku SPD diffractometer at beamline BL-8B of the Photon Factory, KEK, Japan. The wavelength of the synchrotron X-ray was 1.537(1) Å. TEM was performed using a JEOL JEM-2010x electron microscope (200 kV). SEM-EDS analysis was

performed using Phenom World Phenom Pro-x scanning electron microscope (15 kV).

Photocatalytic hydrogen evolution reactions

Under dark conditions, an aqueous solution of KI (0.5 or 0.02 M) and hydrochloride (pH = 2) or phosphate pH buffer (0.5 M, pH = 2) containing Ru(II)-dye-immobilized nanoparticles (100 μM of the Ru(II) dye) was placed into a homemade Schlenk flask-equipped quartz cell (volume: 265 mL) with a small magnetic stirring bar. Each sample flask was doubly sealed with rubber septa. This mixed solution was deoxygenated by Ar bubbling for 1 h. The flask was then irradiated from the bottom with a blue LED lamp (λ = 470 ± 10 nm; 70 mW; Opto Device Lab. Ltd., OP6-4710HP2). The temperature was controlled at 293 K using a homemade aluminum water-cooling jacket with a water-circulating temperature controller (EYELA CCA-1111). The gas samples (0.6 mL) for each analysis were collected from the headspace using a gastight syringe (Valco Instruments Co. Inc.). The amount of evolved H_2 was determined using a gas chromatograph (Agilent 490 Micro Gas Chromatograph). The turnover number and turnover frequency per Ru dye (PS TON/TOF) were estimated from the amount of evolved H_2; two photoredox cycles of the Ru(II) PS are required to produce one H_2 molecule. Each photocatalytic H_2 evolution reaction was conducted under the same conditions three times, and the average value with standard deviation is reported. The detection limit of this gas chromatography analysis for H_2 gas was 0.005 μmol. The AQY was calculated using the following equation:

$$AQY = Ne/Np = 2N_{H2}/Np,$$

Here, Ne represents the number of reacted electrons, N_{H2} is the number of evolved H_2 molecules, and Np is the number of incident photons.

Acknowledgements

The authors thank Mr Tsunenari, Mr. Yamashita and Prof. Y. Hasegawa (Hokkaido Univ.) for valuable support with the SEM-EDS and TEM measurements. This study was supported by the ENEOS Hydrogen Trust Fund, and JSPS KAKENHI, Grant Numbers JP18K19086, JP17H06367, and JP20H05082.

Keywords: Nanoparticles • Photocatalysis • Redox mediator • Surface modification • Water splitting

[1] M. Grätzel, *Acc. Chem. Res.* **1981**, *14*, 376-384.
[2] A. Kudo, Y. Miseki, *Chem. Soc. Rev.* **2009**, *38*, 253-278.
[3] Y. Ma, X. Wang, Y. Jia, X. Chen, H. Han, C. Li, *Chem. Rev.* **2014**, *114*, 9887-10043.
[4] T. Hisatomi, K. Domen, *Nat. Cat.* **2019**, *2*, 387-399.
[5] X. Fang, S. Kalathil, E. Reisner, *Chem. Soc. Rev.* **2020**, *49*, 4926-4952.
[6] A. Fujishima, K. Honda, *Nature* **1972**, *238*, 37-38.
[7] R. Abe, M. Higashi, K. Domen, *ChemSusChem* **2011**, *4*, 228-237.
[8] T. Takata, J. Jiang, Y. Sakata, M. Nakabayashi, N. Shibata, V. Nandal, K. Seki, T. Hisatomi, K. Domen, *Nature*, **2020**, *581*, 411-414.
[9] Z. Song, T. Hisatomi, S. Chen, Q. Wang, G. Ma, S. Li, X. Zhu, S. Sun, K. Domen, *ChemSusChem* **2019**, *12*, 1906-1910.
[10] H. Lyu, T. Hisatomi, Y. Goto, M. Yoshida, T. Higashi, M. Katayama, T. Takata, T. Minegishi, H. Nishiyama, T. Yamada, Y. Sakata, K. Asakura, K. Domen, *Chem. Sci.* **2019**, *10*, 3196-3201.
[11] D. Xu, P. Xu, Y. Zhu, W. Peng, Y. Li, G. Zhang, F. Zhang, T. E. Mallouk, X. Fan, *ACS Appl. Mater. Interfaces* **2018**, *10*, 2810-2818.
[12] A. Vijeta, E. Reisner, *Chem. Comm.* **2019**, *55*, 14007-14010.
[13] L. Yao, A. Rahmanudin, N. Guijarro, K. Sivula, *Adv. Energy Mater.* **2018**, 8, 1802585-1802602.
[14] F. Zhang, Z. Yao, Y. Guo, Y. Li, J. Bergstrand, C. J. Brett, B. Cai, A. Hajian, Y. Guo, X. Yang, J. M. Gardner, J. Widengren, S. V. Roth, L. Kloo, L. Sun, *J. Am. Chem. Soc.* **2019**, *141*, 19700-19707.
[15] Gurudayal, D. Sabba, M. H. Kumar, L. H. Wong, J. Barber, M. Grätzel, N. Mathews, *Nano Lett.* **2015**, *15*, 3833-3839.
[16] K. Maeda, G. Sahara, M. Eguchi, O. Ishitani, *ACS Catal.* **2015**, *5*, 1700-1707.
[17] K. Morita, K. Sakai, H. Ozawa, *ACS Appl. Energy Mater.* **2019**, *2*, 987-992.
[18] B. N. DiMarco, R. N. Sampaio, E. M. James, T. J. Barr, M. Bennett, G. J. Meyer, *ACS Appl. Mater. Interfaces* **2020**, *12*, 23923-23930.
[19] D. Wang, J. Hu, B. D. Sherman, M. V. Sheridan, L. Yan, C. J. Dares, Y. Zhu, F. Li, Q. Huang, W. You, T. J. Meyer, *Proc. Natl. Acad. Sci. U.S.A.* **2020**, *117*, 13256-13260.
[20] P. Xu, T. E. Mallouk, *J. Phys. Chem. C* **2019**, *123*, 299-305.
[21] J. Nomrowski, X. Guo, O. S. Wenger, *Chem. Eur. J.* **2018**, *24*, 14084-14087.
[22] Y. B. M'Barek, T. Rosser, J. Sum, S. Blanchard, F. Volatron, G. Izzet, R. Salles, J. Fize, M. Koepf, M. C.-Kerlidou, V. Artero, A. Proust, *Appl. Energy Mater.* **2020**, *3*, 163-169.
[23] S. Lyu, J. Massin, M. Pavone, A. B. M.-García, C. Labrugère, T. Toupance, M. C.-Kerlidou, V. Artero, C. Olivier, *ACS Appl. Energy Mater.* **2019**, *2*, 4971-4980.
[24] L. Tian, J. Föhlinger, Z. Zhang, P. B. Pati, J. Lin, T. Kubart, Y. Hua, J. Sun, L. Kloo, G. Boschloo, L. Hammarström, H. Tian, *Chem. Comm.* **2018**, *30*, 3739-3742.
[25] B. P. Rimgard, J. Föhlinger, J. Peterson, M. Lundberg, B. Zietz, A. M. Woys, S. A. Miller, M. R. Wasielewski, L. Hammarström, *Chem. Sci.* **2018**, *41*, 7958-7967.
[26] D. M. Fabian, S. Hu, N. Singh, F. A. Houle, T. Hisatomi, K. Domen, F. E. Osterloh, S. Ardo, *Energy Environ. Sci.* **2015**, *8*, 2825-2850.
[27] S. Chen, T. Takata, K. Domen, *Nat. Rev. Mater.* **2017**, *2*, 17050.
[28] R. Abe, K. Shinmei, N. Koumura, K. Hara, B. Ohtani, *J. Am. Chem. Soc.* **2013**, *135*, 16872-16884.
[29] C. Windle, H. Kumagai, M. Higashi, R. Brisse, S. Bold, B. Jousselme, M. Chavarot-Kerlidou, K. Maeda, R. Abe, O. Ishitani, V. Artero, *J. Am. Chem. Soc.* **2019**, *141*, 9593-9602.
[30] K. Koshiba, K. Yamauchi, K. Sakai, *ChemElectroChem*, **2019**, *6*, 2273-2281.
[31] K. Yamamoto, A. Call, K. Sakai, *Chem. Eur. J.* **2018**, *24*, 16620-16629.
[32] S. Sebata, S. Takizawa, N. Ikuta, S. Murata, *Dalton Trans.* **2019**, *48*, 14914-14925.
[33] L. M. Antill, S. Takizawa, S. Murata, J. R. Woodward, *Mol. Phys.* **2019**, *117*, 2594-2603.
[34] S. Takizawa, N. Ikuta, F. Zeng, S. Komaru, S. Sebata, S. Murata, *Inorg. Chem.* **2016**, *55*, 8723-8735.
[35] H. Yang, X. Li, R. S. Sprick, A. I. Cooper, *Chem. Comm.* **2020**, *56*, 6790-6793.
[36] A. Nakada, T. Uchiyama, N. Kawakami, S. Nishioka, R. Kamata, H. Kumagai, O. Ishitani, Y. Uchimoto, K. Maeda, *ChemPhotoChem* **2019**, *3*, 37-45.
[37] M. V. Sheridan, Y. Wang, D. Wang, L. T.-Gautier, C. J. Dares, B. D. Sherman, T. J. Meyer, *Angew. Chem., Int. Ed.* **2018**, *57*, 3449-3453.
[38] Y. I. Kim, S. J. Atherton, E. S. Brigham, T. E. Mallouk, *J. Phys. Chem.* **1993**, *97*, 11802-11810.
[39] R. Abe, K. Shinmei, N. Koumura, K. Hara, B. Ohtani, *J. Am. Chem. Soc.* **2013**, *135*, 16872-16884.
[40] T. Oshima, S. Nishioka, Y. Kikuchi, S. Hirai, K. Yanagisawa, M. Eguchi, Y. Miseki, T. Yokoi, T. Yui, K. Kimoto, K. Sayama, O. Ishitani, T. E. Mallouk, K. Maeda. *J. Am. Chem. Soc.* **2020**, *142*, 8412-8420.
[41] S. Furugori, A. Kobayashi, A. Watanabe, M. Yoshida, M. Kato, *ACS Omega*, **2017**, *2*, 3901-3912.
[42] N. Yoshimura, A. Kobayashi, M. Yoshida, M. Kato, *Bull. Chem. Soc. Jpn.* **2019**, *92*, 1793-1800.

[43] N. Yoshimura, A. Kobayashi, W. Genno, T. Okubo, M. Yoshida, M. Kato, *Sustain. Energy Fuels* **2020**, *4*, 3450-3457.
[44] K. Hanson, M. K. Brennaman, A. Ito, H. Luo, W. Song, K. A. Parker, R. Ghosh, M. R. Norris, C. R. K. Glasson, J. J. Concepcion, R. Lopez, T. J. Meyer, *J. Phys. Chem. C* **2012**, *116*, 14837-14847.
[45] L.T. Gautier, M. D. Turlington, S. A. M. Wehlin, A. B. Maurer, M. D. Brady, W. B. Swords, G. J. Meyer, *Chem. Rev*. **2019**, *119*, 4628-4683.
[46] L.T. Gautier, W. B. Swords, G. J. Meyer, *Acc. Chem. Res.* **2019**, *52*, 170-179.
[47] K. Hu, R. N. Sampaio, J. Schneider, L. Troian-Gautier, G. J. Meyer, *J. Am. Chem. Soc.* **2020**, Accepted. DOI: 10.1021/jacs.0c04886
[48] H. Park, W Choi, M. R. Hoffman, *J. Mater. Chem*. **2008**, *18*, 2379-2385.
[49] M. R. Norris, J. J. Conception, C. R. K. Glasson, Z. Fang, A. M. Lapides, D. L. Ashford, J. L. Templeton, T. J. Meyer, *Inorg. Chem.* **2013**, *52*, 12492-12501.

Entry for the Table of Contents

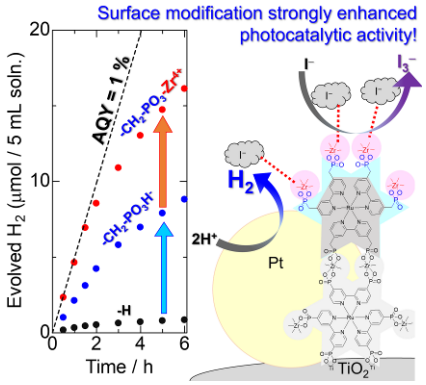

We have systematically modified the surface of double-photosensitizer-layered Pt-cocatalyst-loaded TiO_2 nanoparticles to improve the charge-separation efficiency at the solid–solution interface. The photocatalytic H_2 evolution activity in the presence of redox-reversible iodide electron donors was remarkably improved by the introduction of phosphonates or Zr^{4+}-phosphonate groups on the nanoparticle surface, suggesting that the surface structure is a key factor in achieving one-way electron donation from redox mediators.